

## Increased Elemental Specificity of Positron Annihilation Spectra

P. Asoka-Kumar,<sup>1</sup> M. Alatalo,<sup>1</sup> V. J. Ghosh,<sup>1</sup> A. C. Kruseman,<sup>2</sup> B. Nielsen,<sup>1</sup> and K. G. Lynn<sup>1</sup>

<sup>1</sup>Brookhaven National Laboratory, Upton, New York 11973

<sup>2</sup>IRI, Delft University of Technology, Mekelweg 15, NL-2629JB Delft, The Netherlands

(Received 28 March 1996)

Positron annihilation spectroscopy (PAS) is a sensitive probe for studying the electronic structure of defects in solids. We show that the high-momentum part of the Doppler-broadened annihilation spectra can be used to distinguish different elements. This is achieved by using a new two-detector coincidence system to examine the line shape variations originating from high-momentum core electrons. Because the core electrons retain their atomic character even when atoms form a solid, these results can be directly compared to simple theoretical predictions. The new approach adds increased elemental specificity to the PAS technique, and is useful in studying the elemental variations around a defect site. [S0031-9007(96)01120-9]

PACS numbers: 78.70.Bj, 71.60.+z

Positron annihilation spectroscopy (PAS) is a sensitive probe for studying defects in solids [1,2]. The method relies on the propensity of positrons to become localized at open-volume regions of a solid and the emission of annihilation gamma rays that escape the test system without any final state interaction. These gamma rays hold information about the electronic environment around the annihilation site. PAS measurements for defect characterization generally utilize two observables: positron lifetime and the conventional Doppler broadening of the annihilation gamma rays using a single detector. Both of these techniques are not very sensitive to elemental variations around an annihilation site, such as the one occurring when a material is lightly doped with another or when a vacancy is tied with an impurity atom. A third observable, angular correlation of annihilation radiation, can overcome this deficiency. However, this observable is not used routinely in defect spectroscopy owing to the difficulties associated with the low counting rates at many of the existing facilities. Here we present the results from a new two-detector setup that measures the elemental variations around the annihilation site. The new setup improves the peak to background ratio in the annihilation spectrum to  $\sim 10^5$ , and as a result the variations of the Doppler-broadened spectra resulting from annihilations with different core electrons can be mapped. Because the core electrons retain their atomic character even when atoms form a solid, the new results can be easily verified with straightforward theoretical calculations. In the past, Lynn *et al.* have shown the advantage of using a two-detector setup in a study of thermal generation of vacancies in aluminum [3,4].

Upon entering the solid, positrons lose most of their kinetic energy and reach thermal equilibrium with the host material (within about 10 psec). In a crystal, the thermalized positrons experience a periodic repulsive potential that is centered on the ionic cores, and their wave function is confined to the interstitial region. Their subsequent mo-

tion is dominated by phonon scattering, and in the absence of an overall electric field in the medium, this motion is nearly an isotropic random walk. Open-volume defects and negative charge centers provide isolated minima in the potential and localize positrons. Eventually positrons, localized at defects or not, annihilate with electrons producing predominantly two gamma rays, necessitated by energy-momentum conservation during annihilation. Because the positrons are thermalized, the total energy of the annihilation gamma rays is given by  $2m_0c^2 - E_B$ , where  $m_0c^2$  is the electron rest mass energy and  $E_B$  is the electron binding energy (neglecting the thermal energies and chemical potentials). When there is a net center of mass energy associated with the annihilating pair, this total energy is not split equally among the two gamma rays. One gamma ray is upshifted while the other is downshifted from the center energy of  $m_0c^2 - E_B/2$  by an amount given by  $\Delta E = (1/2)p_Lc$ , where  $p_L$  is the longitudinal component of the electron-positron momentum along the direction of the gamma ray emission. Since the direction of the gamma ray emission is random, a detector located in a given direction will record both upshifted and downshifted gamma rays. This produces an overall Doppler broadening, and characterizing this broadening provides a sensitive way of examining the electronic environment around the annihilation site.

Annihilations with core electrons produce larger Doppler shifts compared to valence electrons. Therefore, the tail region of the Doppler-broadened curve can be analyzed to obtain the momentum distribution of the core electrons. In traditional Doppler-broadening measurements, a single detector records the energy of the annihilation gamma rays. The spectrum collected with a single detector suffers from high background contributions (peak to background ratio  $\sim 200$ ), which arise mostly from incomplete charge collection on the low energy side and pileup and sum events on the high energy side. When positronium is formed, annihilation into three

gamma rays also can contribute to the low energy side. As a result, the line shape variations arising from the contribution of the core electrons cannot be easily extracted. On the other hand, if the energies of both gamma rays (from each annihilation event) are recorded, the signal to background ratio can be dramatically improved in the tail region.

Figure 1 shows a two-dimensional spectrum recorded with a 30 keV positron beam striking a Si(100) target. For every coincident event, the energies of both gamma rays (denoted by  $E_1$  and  $E_2$ ) are registered in two high purity Ge detectors arranged at  $180^\circ$  to each other. These energies form the horizontal and vertical axes, and the count corresponding to each  $E_1$  and  $E_2$  combination is indicated in color, depending on their absolute values. There is an intense central peak centered at  $E_1 = E_2 = 511$  keV, which corresponds to annihilations with the valence electrons. On either side of this central peak, the spectrum shows horizontal and vertical bands. The low energy bands (horizontal with  $E_1 < 511$  keV or vertical with  $E_2 < 511$  keV) are produced mostly by events in which one Ge detector records a photon in the photopeak, while the other records the energy of the second photon (from the same annihilation event) at a lower value due to incomplete charge collection. Typical absolute photopeak efficiency of the detectors used for these measurements is  $\sim 0.2\%$  at 511 keV at a source-detector distance of 25 cm. The high energy bands (horizontal with  $E_1 > 511$  keV or vertical with  $E_2 > 511$  keV) correspond to an event in which one detector records the gamma ray energy in the photopeak and the other records a piled-up event. The elliptical region extending diagonally with  $E_1 + E_2 \approx 2m_0c^2 = 1022$  keV originates from annihilations with high momentum electrons, and this region is nearly background free. A cut along the diagonal can then

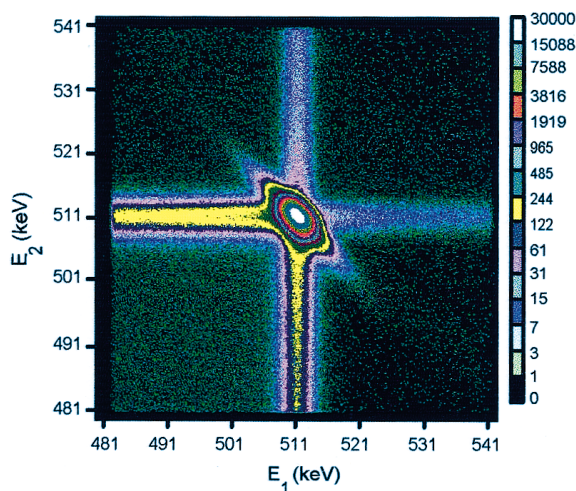


FIG. 1(color). A two-dimensional display of coincident events collected with a Si(100) target. The spectrum contains a total of  $15 \times 10^6$  events.

be analyzed to observe variations in shape due to the contributions of core electrons.

In Fig. 2, we show the results obtained with a traditional setup using a single Ge detector and a two-detector coincidence system. The coincidence result corresponds to a projection onto  $E_1 - E_2$  ( $= 2\Delta E = p_L c$ ) axis from Fig. 1. The projection includes events in a window along the diagonal with  $2m_0c^2 - 2.4$  keV  $< E_1 + E_2 < 2m_0c^2 + 2.4$  keV. The width of the sum-energy window is selected to exclude horizontal and vertical bands depicted in Fig. 1 and to include regions corresponding to the deficit in sum energies arising out of electron binding energies. Increasing the sum-energy window to  $2m_0c^2 \pm 4.8$  keV did not change the shape of the annihilation spectrum, apart from an increase in the background. The plot reveals the increased sensitivity of the new method to high momentum contributions. As shown, a small improvement can also be made with a single Ge detector in coincidence with a  $\gamma$ -ray detector (such as a NaI detector). Recently this later approach has been used by some authors [5–7].

Figure 2 also compares results for Si and Ge and shows shape variations arising from core annihilations. The samples used in the present study are high-purity single crystals and are “defect free” as seen by positrons. The spectra correspond to an incident positron beam energy of 30 keV and correspond to a mean penetration depth of  $\sim 4 \mu\text{m}$  in Si and  $\sim 1.7 \mu\text{m}$  in Ge, deep enough to exclude ( $< 1\%$ ) positron diffusion to the surface and subsequent annihilation from the surface states. Since the spectrum is symmetric with respect to  $E_1 - E_2 = 0$ ,

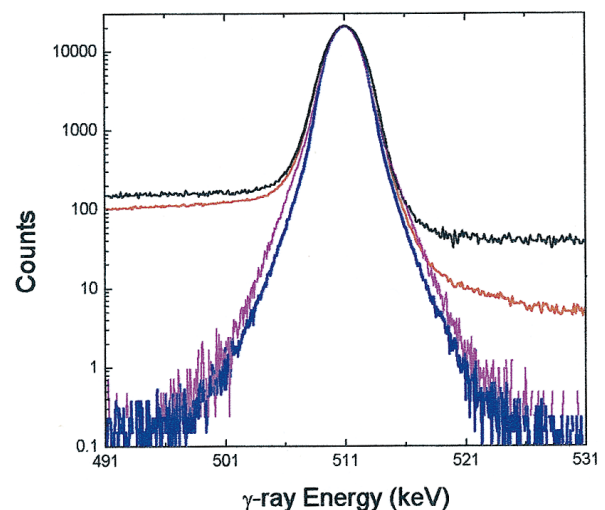


FIG. 2(color). The comparison of the Doppler-broadened spectrum of Si collected with three different arrangements: a single detector (black), a single detector in coincidence with a NaI detector (red), and two detectors in coincidence (blue). The difference between the two coincident arrangements is that in the first case the energy of only one of the  $\gamma$  rays is recorded. The plot also includes data from Ge (magenta).

the next figure displays the results by folding it about  $E_1 - E_2 = 0$  and averaging.

As already discussed in Ref. [7], the larger amplitude of the Ge curve stems from the fact that the outermost core shell in the case of Ge is  $3d$ , which is highly occupied and spatially extended. Therefore the annihilation rate with  $3d$  electrons in Ge is high. Being rather localized in  $r$  space,  $3d$  electrons produce a wide distribution in the momentum space. This is better seen in Fig. 3, where we present the experimental data for Al, Si, and Ge, together with the theoretical curves, calculated using a method described in more detail in Ref. [7]. Figure 3 also shows the partial contribution from the individual shells of Ge. The total contribution has been convoluted with the detector resolution.

The momentum distribution for each core electron state is calculated within the independent particle model using free atom wave functions. These individual contributions are then summed up by using state dependent enhancement factors obtained by calculating the positron wave function and the ensuing annihilation rate using the method of superimposed atoms in solving the three-

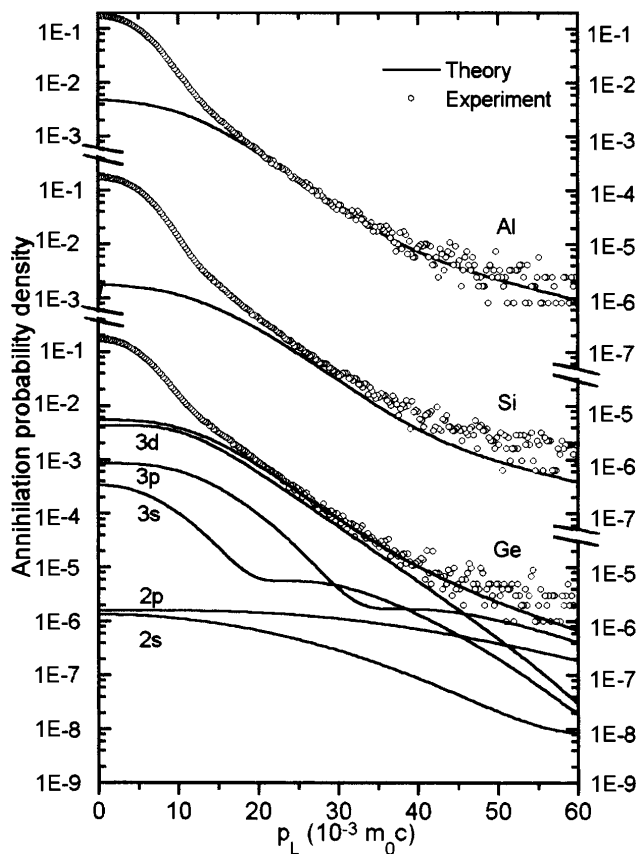


FIG. 3. The comparison of the experimental and theoretical annihilation probability densities for Al, Si, and Ge. The area under the experimental data is normalized to unity. The calculated curves have been normalized to the quantity  $\lambda_c/\lambda_{tot}$ , where  $\lambda_c$  and  $\lambda_{tot}$  are the annihilation rate with core electrons and the total annihilation rate, respectively.

dimensional Schrödinger equation [8]. Since the core electrons retain their atomic character even when atoms form a solid, atomic wave functions provide an accurate description of the core electron states. Atomic wave functions, however, are not an accurate description of the valence electrons. Annihilations with valence electrons produce smaller Doppler shifts ( $\approx 20 \times 10^{-3} m_0 c$ ) than annihilations with core electrons. Since the treatment of the valence electrons is only approximately correct, their contributions to the Doppler broadening is not added to the total. Experimentally, the present approach cannot resolve the partial contributions. However, by detecting the Auger electrons or x rays generated from the core-hole decay in coincidence with the two annihilation photons, these partial contributions can be measured directly.

Since the counts vs energy curves span several orders of magnitude, the shape difference between them can be seen more easily after normalizing the measured spectrum to a reference spectrum. In this Letter, we chose Al as the reference spectrum. Figure 4(a) shows the normalized data set for several elements. The normalization involved the following steps: For each element, the area under the curve (after folding) is normalized to unity. The unity area curves are smoothed (16 point averaging consistent

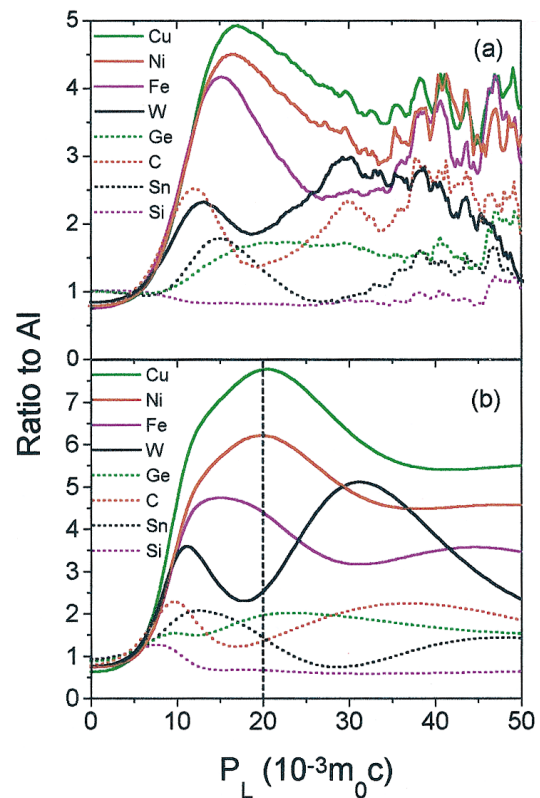


FIG. 4(color). The spectrum for different elements after normalizing to Al: (a) experiment and (b) theory. The theoretical curves for  $p_L < 20 \times 10^{-3} m_0 c$  [dashed line in (b)] are not accurate.

with the system resolution) and divided by the Al curve. Corresponding theoretical curves are shown in Fig. 4(b). Because our calculations do not treat contributions from valence electrons accurately, the theoretical curves below  $20 \times 10^{-3} m_0c$  are not reliable. As can be seen, the agreement between theory and experiment is only qualitative. At high  $p_L$  values, where the theoretical curves show many interesting features, the present experimental values are not reliable due to low statistics. Nevertheless, the theoretical curves also show elemental specificity, and there are some qualitative trends that are worth noticing. For example, both the calculated and experimental curves for W show a valley at  $\sim 20 \times 10^{-3} m_0c$  and a peak (arising from  $4f$  electrons) at  $\sim 32 \times 10^{-3} m_0c$ .

It is interesting to note that there are small differences [ $\sim 20\%$ , Fig. 4(a)] between elements that are adjacent in the periodic table. The difference between Si and Al arises mainly from the different lattice structure. In fcc Al the interstitial space is reduced compared with Si having diamond structure, and therefore the overlap of the positron wave function (which is more confined to the interstitial region due to the Coulomb repulsion of the ionic core) with core electron wave functions is larger. This increase in overlap produces the increase in the ratio curve seen at higher Doppler shifts [ $> 7 \times 10^{-3} m_0c$ , see Fig. 4(a)]. Because of the similar core structure, however, the shape of the core distributions arising from Al and Si is very similar. Therefore, it might be hard to distinguish them in situations such as Si doped with Al. Nevertheless, differences between elements that are not adjacent in the periodic table are significant enough to conclude that the technique can be applied to examine elemental variations around an open-volume defect site, such as an impurity-vacancy complex. In a related study using a single Ge detector in coincidence with a NaI detector, Szpala *et al.* recently showed that the binding of Sb to vacancies in Si can be easily observed [6].

In conclusion, we have shown that a two-detector coincidence system can improve the sensitivity of the positron annihilation measurements. The increased sensitivity compared to the previous Doppler-broadening measurements allows us to extract the chemical identity of the atoms. The method can be used to study a wide variety of problems, like simple open-volume defects, open-volume defects decorated with foreign elements, and vacancies in different sublattices of a stoichiometric compound. We also show that simple theoretical models can be used to interpret these results.

We thank F.M. Jacobsen, M.J. Puska, P. Mijnders, and T. Korhonen for various discussions. This work was supported in part by U.S. DOE under Contract No. DE-AC02-76CH00016. One of us (ACK) thanks the Netherlands Organization for Scientific Research (NWO) for a travel grant.

- 
- [1] P.J. Schultz and K.G. Lynn, *Rev. Mod. Phys.* **60**, 701 (1988).
  - [2] M.J. Puska and R.M. Nieminen, *Rev. Mod. Phys.* **66**, 841 (1994).
  - [3] K.G. Lynn, J.R. MacDonald, R.A. Boie, L.C. Feldman, J.D. Gabbe, M.F. Robbins, E. Bonderup, and J. Golovchenko, *Phys. Rev. Lett.* **38**, 241 (1977).
  - [4] K.G. Lynn, J.E. Dickman, W.L. Brown, M.F. Robbins, and E. Bonderup, *Phys. Rev. B* **20**, 3566 (1979).
  - [5] M. Alatalo, H. Kauppinen, K. Saarinen, M.J. Puska, J. Mäkinen, P. Hautojärvi, and R.M. Nieminen, *Phys. Rev. B* **51**, 4176 (1995).
  - [6] S. Szpala, P. Asoka-Kumar, B. Nielsen, J.P. Peng, S. Hayakawa, K.G. Lynn, and H.-J. Gossmann, *Phys. Rev. B* (to be published).
  - [7] M. Alatalo, B. Barbiellini, M. Hakala, H. Kauppinen, T. Korhonen, M.J. Puska, K. Saarinen, P. Hautojärvi, and R.M. Nieminen, *Phys. Rev. B* **54**, 2397 (1996).
  - [8] M.J. Puska and R.M. Nieminen, *J. Phys. F* **13**, 333 (1983).